Large Equatorial Ligand Effects on C–H Bond Activation by Nonheme Iron(IV)–oxo Complexes

ARTICLE *in* THE JOURNAL OF PHYSICAL CHEMISTRY B · JANUARY 2014

Impact Factor: 3.3 · DOI: 10.1021/jp410727r · Source: PubMed

THE JOURNAL OF PHYSICAL CHEMISTRY B

Article

pubs.acs.org/JPCB

Large Equatorial Ligand Effects on C−H Bond Activation by Nonheme Iron(IV)-oxo Complexes

Xiaoli Sun,[†,∥] Caiyun Geng,[†,∥] Ruiping Huo,[†] Ulf Ryde,[§] Yuxiang Bu,[‡] and Jilai Li*[,†,§]

[†]State Key Lab of Theoretical and Computational Chemistry, Institute of Theoretical Chemistry, Jilin University, Liutiao Road 2, Changchun 130023, People's Republic of China

[‡]School of Chemistry and Chemical Engineering, Shandong University, Jinan 250100, People's Republic of China

[§]Department of Theoretical Chemistry, Lund University, Chemical Center, SE-221 00 Lund, Sweden

Supporting Information

ABSTRACT: In this article, we present density functional theory (DFT) calculations on the iron(IV)-oxo catalyzed methane C−H activation reactions for complexes in which the Fe^{IV}═O core is surrounded by five negatively charged ligands. We found that it follows a hybrid pathway that mixes features of the classical σ- and π-pathways in quintet surfaces. These calculations show that the Fe−O−H arrangement in this hybrid pathway is bent in sharp contrast to the collinear character as observed for the classical quintet σ-pathways before. The calculations have also shown that it is the equatorial ligands that play key roles in tuning the reactivity of Fe^{IV}═O complexes. The strong π-donating equatorial ligands employed in the current study cause a weak π(FeO) bond and thereby shift the electronic accepting orbitals (EAO) from the vertically orientated O p_z orbital to the horizontally orientated O p_x. In addition, all the equatorial ligands are small in size and would therefore be expected have small steric effects upon substrate horizontal approaching. Therefore, for the small and strong π-donating equatorial ligands, the collinear Fe−O−H arrangement is not the best choice for the quintet reactivity. This study adds new element to iron(IV)-oxo catalyzed C−H bond activation reactions.

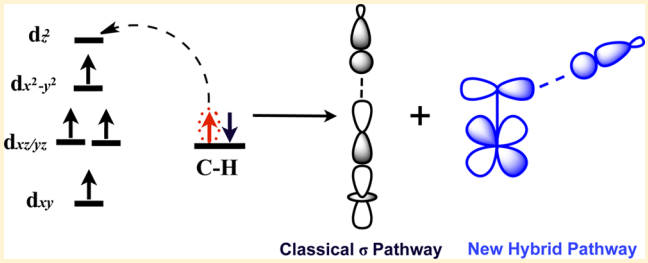

INTRODUCTION

The transformation of the ubiquitous but inert C−H bond to functional groups has far-reaching practical implications and it has been studied for over 100 years.[1−4] High-valent iron(IV)-oxo species have been implicated as the key intermediates in the catalytic cycles of heme and nonheme oxygen activating iron enzymes that selectively functionalize aliphatic C−H bonds.[5−15] Significant progress in understanding of the electronic and spectroscopic properties of these compounds, and how they react with C−H bonds in these enzymatic reactions has been done via both experimental and theoretical investigations.[9−45] However, continued extensive research is still needed to clarify the currently unanswered questions in both enzymatic and biomimetic reactions.

Iron has several available spin states and much interest has been devoted to the different reactivity of C−H bond activation by each spin state.[31−34] For nonheme systems, iron(IV)-oxo intermediates are known to exist in either triplet or quintet ground states. In most studies, two reaction pathways have been established, a σ-mechanism for the quintet and a π-mechanism for the triplet (Scheme 1A,B).[14−16] These two reaction pathways differ in energy barriers and geometric features during the C−H bond activation. In the quintet σ-pathway, an α-electron from the substrate is shifted toward the Fe $3d_{z^2}$ orbital and therefore features a nearly collinear Fe−O−H arrangement in the transition state (Scheme 1A). In contrast, the triplet π-pathway is characterized by a equatorial approach of the substrate that shifts a β-electron from the substrate to the Fe $3d_{xz}$ orbital and features a bent Fe−O−H arrangement in transition state (Scheme 1B). According to density functional theory (DFT) calculations, the reactivity toward C−H bond cleavage is much higher for the quintet iron(IV)-oxo intermediates than for the corresponding triplet species.[7,10,16,45−48]

Recently, mechanistic studies of C−H bond activation by the Solomon and Neese groups have made the picture more complete. Solomon and co-workers revealed a new reaction pathway on the quintet surface in an intramolecular benzylic C−H bond activation by 4-hydroxymandelate synthase.[49] They found that this new quintet pathway leads to a shift of a β- rather than an α-electron into the π^*(FeO) orbital and correspondingly, a bent Fe−O−H arrangement rather than a collinear arrangement is established in the transition states. These are quite similar as those found in the π-pathway for the triplet surface. Moreover, Neese and co-workers have done a thorough theoretical study of all possible reaction pathways in C−H bond activation for ferryl model complexes.[28] With the free substrates, they identified two additional pathways besides

Received: October 30, 2013
Revised: January 27, 2014
Published: January 28, 2014

   dx.doi.org/10.1021/jp410727r | J. Phys. Chem. B 2014, 118, 1493−1500

Scheme 1. Schematic Representation of the Feasible Reaction Channels for the C−H Activation by Iron(IV)-oxo Complexes[a]

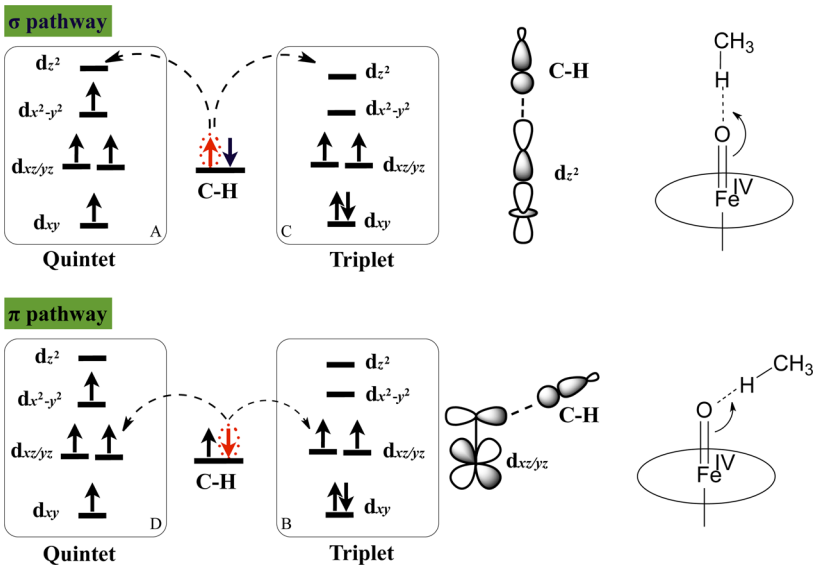

[a]DFT calculations have demonstrated that the barrier heights follow the order ${}^5\sigma < {}^5\pi \approx {}^3\pi < {}^3\sigma$.[28]

the two classical pathways mentioned above (Scheme 1A,B), they identified two additional pathways, viz. a σ-pathway for triplet state and a π-pathway for quintet state (Scheme 1C,D). In fact, they found that the reactivity of the new quintet π-pathway was comparable or even higher than that of the classical triplet π-pathway.[28] All these researches indicated that there should exist two kinds of attack modes for the substrates approaching the active center, either for the triplet or quintet states. These two attack modes are closely related to the reaction mechanisms, that is, the horizontal attack is corresponding to the π-mechanism, while the vertical attack is related to the σ-mechanism. The picture for the C−H bond activation by nonheme complexes seems complete.

Another focus of current research is the role of the axial ligand in the reactivity of iron(IV)-oxo species and the results indicate that it is a major determinant for the C−H activation reactivity.[10,41,50−56] This hypothesis was originally inspired from the different catalytic ability of heme enzymes and it has been extended to the nonheme field.[48] From DFT studies, Baerends proposed a "push effect" of σ-donating axial ligands and established a linear relationship between the σ-donor properties of the axial ligands and the activation barrier for the abstraction reactions.[21] Recently, the axial ligand effect has been analyzed using thermodynamic cycles developed by Bordwell et al. and others.[57,58] Within this framework, the effect of the axial ligand can be rationalized by the redox potential of the M = O oxidant and the pK_a of the nascent O−H bond.[58] These studies demonstrated the importance of the axial ligand in dictating the reactivity of metal−oxo species toward C−H bond activation.[10] However, little effort has been directed toward the influence of equatorial ligands in the reactivity of iron(IV)-oxo complexes.[50,56]

In this paper, we study the iron(IV)-oxo catalyzed methane C−H activation reactions for complexes in which the Fe^{IV}=O core is surrounded by five negatively charged ligands. We analyze the reaction pathways in the simple $[Fe^{IV}(O)(CN)_5]^{3-}$ model and then gradually substitute the CN^- ligands with NC^- or F^- ligands (Scheme 2). We study whether these strongly negatively charged compounds have a similar reactivity as

Scheme 2. A Schematic Representation of the Studied Fe^{IV}-oxo Model Complexes[a]

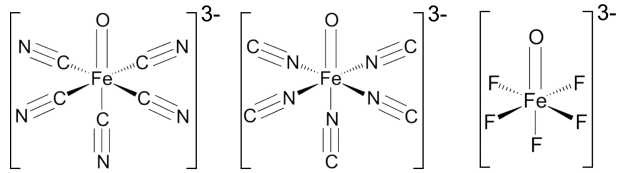

[a]Left $[Fe^{IV}(O)(CN)_5]^{3-}$; middle $[Fe^{IV}(O)(NC)_5]^{3-}$; right $[Fe^{IV}(O)(F)_5]^{3-}$. All the other model complexes are shown in the Supporting Information.

previously studied models: (1) Can the same four reactions pathways be found for these reactions? (2) Do the transition states of the σ- and π-mechanisms have the same structures? (3) How do the equatorial ligands modulate the reactivity of these iron(IV)-oxo species? The calculations have allowed us to gain atomistic insight into catalytic reactivity of these high-valent oxoiron complexes and shed light on how new reagents may modify C−H bonds with high efficiency and specificity.

METHODS

All calculations were performed with the ORCA package.[59] The hybrid B3LYP density functional was employed in all calculations.[60,61] It is the most widely used density functional and it has a well-documented accuracy. For molecules containing first- and second-row atoms, the errors are seldom higher than 13 kJ/mol, and for transition-metal biochemistry the accuracy is normally within 21 kJ/mol.[45]

All of the geometries were fully optimized without symmetry constraints. Harmonic vibrational frequencies were computed to verify the nature of the stationary points. The minimum structures reported in this paper show only positive eigenvalues of the Hessian matrix, whereas the transition states (TSs) have only one negative eigenvalue. Zero-point energies, as well as entropy and thermal corrections to the Gibbs free energy at 300 K and 1 atm pressure were obtained from the frequencies using

dx.doi.org/10.1021/jp410727r | J. Phys. Chem. B 2014, 118, 1493−1500

Table 1. Key Geometric Parameters, Activation Enthalpies, and the Percentages of the π-Components in the Molecular Orbital of Fe^{IV}=O Core in Reactant States for the New Quintet Hybrid Pathway

model[a]	state[b]	Fe−O[c]	O−H[c]	C−H[c]	∠FeOH[d]	TS[e]	Oπ_1[f]	Oπ_2[f]	Feπ_1[f]	Feπ_2[f]
5C	^{5}TSHh	1.81	1.14	1.37	132.9	43.2	62.4	56.8	37.2	42.2
	^{3}TSHπ	1.82	1.11	1.45	116.0	21.8				
5N	^{5}TSHh	1.84	1.22	1.27	123.7	13.6	60.9	60.8	39.3	39.4
	^{3}TSHπ	1.79	1.14	1.40	115.5	18.5				
5F	^{5}TSHh	2.03	1.19	1.29	108.5	7.9	73.8	74.0	26.9	26.7
	^{3}TSHπ	1.80	1.01	1.89	109.6	34.7				
4C-1N	^{5}TSHh	1.83	1.17	1.32	129.2	39.6	64.1	57.8	35.6	41.5
	^{3}TSHπ	1.80	1.11	1.45	116.2	23.1				
3C-2N	^{5}TSHh	1.81	1.16	1.35	133.8	28.7	64.3	51.4	35.9	47.4
	^{3}TSHπ	1.82	1.12	1.42	116.1	20.1				
2C-3N	^{5}TSHh	1.82	1.17	1.32	130.7	25.2	53.1	65.6	45.9	34.8
	^{3}TSHπ	1.79	1.12	1.42	116.1	21.4				
1C-4N	^{5}TSHh	1.82	1.19	1.30	130.1	15.9	59.3	59.3	40.8	40.7
	^{3}TSHπ	1.81	1.14	1.39	114.9	17.4				
4C-1F	^{5}TSHh	1.85	1.18	1.32	127.4	33.1	64.5	64.5	35.2	35.2
	^{3}TSHπ	1.81	1.09	1.49	116.4	23.4				
3C-2F	^{5}TSHh	1.91	1.21	1.28	115.6	16.3	74.1	56.3	26.4	43.7
	^{3}TSHπ	1.83	1.10	1.47	116.9	22.0				
2C-3F	^{5}TSHh	1.94	1.20	1.29	114.4	13.7	64.1	74.0	35.5	26.7
1C-4F	^{5}TSHh	1.98	1.20	1.29	110.0	8.3	72.4	72.5	28.3	28.2
4N-1F	^{5}TSHh	1.86	1.22	1.27	121.3	12.7	63.4	63.6	36.9	36.7
	^{3}TSHπ	1.79	1.12	1.42	115.4	23.8				
3N-2F	^{5}TSHh	1.90	1.22	1.27	113.6	12.5	72.1	60.2	28.7	39.8
	^{3}TSHπ	1.80	1.12	1.44	117.1	31.2				
2N-3F	^{5}TSHh	1.93	1.21	1.28	114.6	13.5	71.9	63.3	29.1	36.8
	^{3}TSHπ	1.79	1.10	1.49	115.1	36.1				
5A[g]	^{5}TSHσ	1.73	1.24	1.28	179.3	10.5	58.3	59.2	42.3	41.4

[a]As shown in Supporting Information Scheme S1, the models contain Fe(IV), oxo (O), and five ligands, which are either CN^- (C), NC^- (N), F^- (F), or NH_3 (A). [b]The pathways. [c]The bond distance (Å). [d]The Fe−O−H angle (°). [e]The activation enthalpy (kcal/mol). [f]The π-components of Fe=O core molecular orbital in the reactant state. [g]For comparison, we also include results of the classical quintet σ-pathway for $[Fe^{IV}(O)(NH_3)_5]^{2+}$.[28] The complete table for all pathways is shown in Supporting Information.

an ideal-gas rigid-rotor harmonic-oscillator approximation. In all calculations, we used tight SCF convergence criteria and finer-than-default integration grids (Grid4 in ORCA) in order to get fully converged stationary points with accurate energies on the minimum-energy pathways.

All structures were optimized with the triple-ζ quality def2-TZVP basis sets.[62] The density-fitting (resolution-of-the-identity approximation) and chain-of-sphere techniques, RIJCOSX[63] approximation were used for the Coulomb and HF exchange terms in B3LYP to accelerate the calculations using the auxiliary basis sets def2-TZVP/J. More accurate energy calculations were performed with the B3LYP method using the def2-TZVPP basis sets including high angular momentum polarization functions.[64] The RIJCOSX approximation was employed with the def2-TZVPP/J auxiliary basis set.[65]

To take into account the role of solvent effect, the conductor-like screening model (COSMO) was used for all calculations and a common choice of the dielectric constant (ε = 4) was chosen to mimic a protein-like environment.[66] Given the deficiencies of DFT in modeling the London dispersion forces, a dispersion correction of the DFT energy term is important. Therefore, the DFT-D3 dispersion correction proposed by Grimme was used in the final energy calculated by the dftd3 program.[67,68]

It is important to realize that the self-interaction error (SIE) in density functional theory results in artificial stabilization of some states, especially in systems having an odd electron number.[69] Two methods, the solvent correction and counterion are used to remove this error nowadays.[70] In this work, initial test calculations under gas phase were performed. By using implicit COSMO solvent model, the results of electron transfer mechanism and energetics are reliable. Although the solvent effect might not remove the SIE completely, the conclusion of the current study is trustable.

RESULTS AND DISCUSSION

In accordance with previous studies, we find that the C−H bond activation by all these model complexes follows a hydrogen-atom transfer (HAT) mechanism.[14,16,23,28,49,71,72] We could find two pathways for most of the models in the quintet state, as well as the triplet π-pathway (Table S1 in the Supporting Information). However, the triplet σ-pathway could be located in only two systems **3C-2N** and **2C-3N** (the nomenclature of the models is explained in footnote [a] of Table 1) owing to its high activation energy. Considering the large negative charge of the present complexes, which would make them poor electrophiles for C−H bond activation, high barriers could be expected for all these complexes. However, it turned out that the calculated activation enthalpies were unexpectedly low, especially for complexes with F^- ligands. As

dx.doi.org/10.1021/jp410727r | J. Phys. Chem. B 2014, 118, 1493−1500

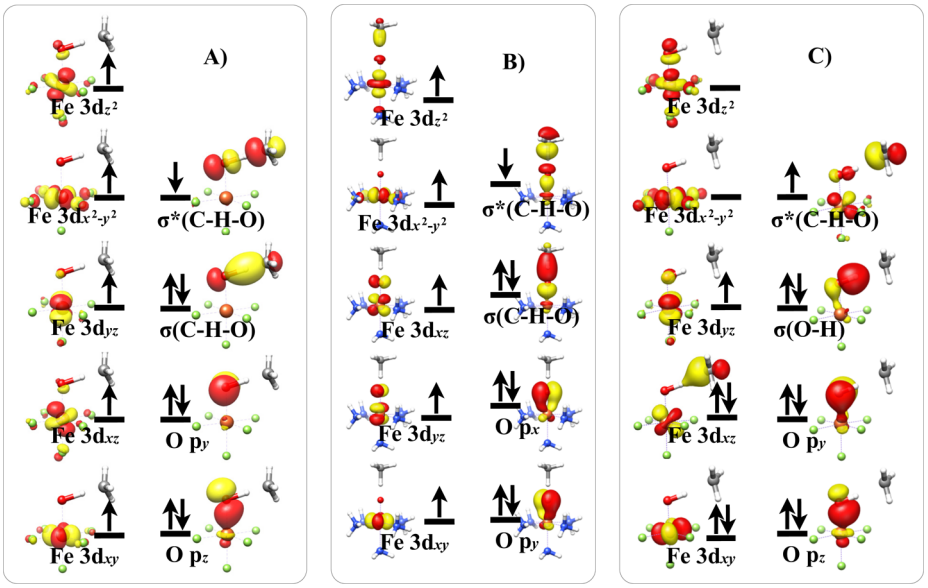

Figure 1. Schematic MO diagram of ^{5}TSHh (A) in the quintet hybrid pathway of $[Fe^{IV}(O)(F)_5]^{3-}$, ^{5}TSHσ (B) in the classical quintet σ-pathway of $[Fe^{IV}(O)(NH_3)_5]^{2+}$, and ^{3}TSH$\pi$ (C) in triplet π of $[Fe^{IV}(O)(F)_5]^{3-}$. F, green; Fe, orange; C, gray; N, blue; and O, red.

is shown in Table 1, the calculated activation barriers for models **5N**, **5F**, **1C-4F**, **1C-4N**, **4N-1F**, **3N-2F**, **3C-2F**, **2N-3F**, and **2C-3F** are all below 17 kcal/mol. In fact, the barrier of **5F** is lower than that of **5A** although the charge is five units more negative.

The calculated structures for the π-pathways for both triplet and quintet surfaces closely resemble those found in previous studies (Table 1).[7,16,28] However, the second pathway which should be deemed as σ pathway for the quintet state exhibits some interesting geometric differences. First, the optimized Fe−O−H angles of the transition stats are not collinear as observed for the quintet σ-pathway in previous studies (illustrated by the **5A** complex).[7,28,70,73,74] As is shown in Table 1, the largest ∠FeOH angle for negatively charged models is 134° (**3C-2N**), far from a collinear arrangement. In fact, ∠FeOH is 124, 105, 99, 116, 108, 121, and 114° for **5N**, **S-5C**, **S-5N** and **3C-2F**, **5F**, **4N-1F** and **3N-2F** systems, which are comparable or even smaller than the corresponding π-pathways. Second, the Fe−O bonds are unexpectedly long. For example, the calculated Fe−O bond length of **5N** system is 1.84 Å, that is, 0.11 Å longer than for that in **5A**, the typical example of a classical quintet σ-pathway, and that for **5F** is even longer, 2.03 Å.

Figure 1 shows schematic MO diagrams for the transition states of this pathway (^{5}TSHh) and triplet π-pathway (^{3}TSHπ) for model **5F**, as well as for the classical quintet σ-pathway of **5A**;[28] corresponding figures for other systems can be found in Figure S1 in the Supporting Information. It can be seen that in ^{5}TSHh, an α-electron from the substrate has moved to the σ^* z^2 orbital of Fe−O moiety, leading to a high-spin (HS) Fe(III) ion (S_{Fe} = 5/2) antiferromagnetically coupled to a three-center C−H−O radical (S_{CHO} = 1/2) (Figure 1A). This electronic state of iron center closely resembles that found in the classical quintet σ-pathway (Figure 1B). However, the σ^*(C−H−O) orbital is the antibonding combination between the σ(C−H) and the O p_x fragment orbitals in the same way as for the π-pathway (Figure 1C), rather than the O p_z orbital that is employed in the classical σ-pathway (Figure 1B).[28] Therefore, the electronic structure of the transition state for this pathway mix features from the classical σ- and π-pathways, and we call it hybrid pathway in our study. The use of the O p_x orbital explains the bent Fe−O−H arrangement in ^{5}TSHh.

To understand the unusual electronic features of this hybrid pathway, we follow the O−H reaction coordinate for CH_4 approaching the Fe−O moiety (Figure 2). As expected from the quintet σ-pathway, the substrate initially approaches the Fe−O moiety vertically, giving a collinear Fe−O−H arrangement (Figure 2A). However, when the O−H distance is shortened below ∼1.3 Å, another electronic state becomes more favorable (Figure 2C). Comparing the two electronic structures in Figure 2, shows that the σ^*(C−H−O) orbital shifts from using the vertically orientated O p_z to the horizontally orientated O p_x, leading to an electronic structure that closely resembles the one found in ^{5}TSHh. To understand why the Fe−O moiety makes such a change in the electronic state when the substrate approaches, we studied the electronic structure of the isolated Fe−O moiety when the Fe−O bond is elongated.[6] This is shown in Figure 3. When the Fe−O bond is elongated less than 1.91 Å, we found that the electronic structure of Fe−O moiety closely resembled those in the previous study (Figure 3B), that is, the σ(FeO) bonding orbital splits into a spin-coupled pair with the spin-up electron residing in the Fe $3d_{z^2}$ orbital and the spin-down MO having O p_z character (Figure 3B).[6] However, we did not stop and continued with further elongation. Surprisingly, we got a new electronic structure at Fe−O bond of 1.92 Å (Figure 3B). In this electronic structure, a horizontal O p_x electron hole rather than the vertical O p_z orbital is generated on the oxo moiety. Maintained with this electronic structure, we carefully shorted and elongated the Fe−O bond and got the smooth red curve shown in Figure 3. It crossed with the black curve at about 1.86 Å. Clearly, the two curves are related to different potential energy surfaces. The black curve is the ground state for the relative short Fe−O bond (<1.86 Å) and the red one favors over the long Fe−O bond (>1.86 Å).

Comparison of the electronic structure of Fe−O species in Figure 3 with that of ^{5}TSHh provides a coherent picture on how the electron transfer from the substrate to the iron center

dx.doi.org/10.1021/jp410727r | J. Phys. Chem. B 2014, 118, 1493−1500

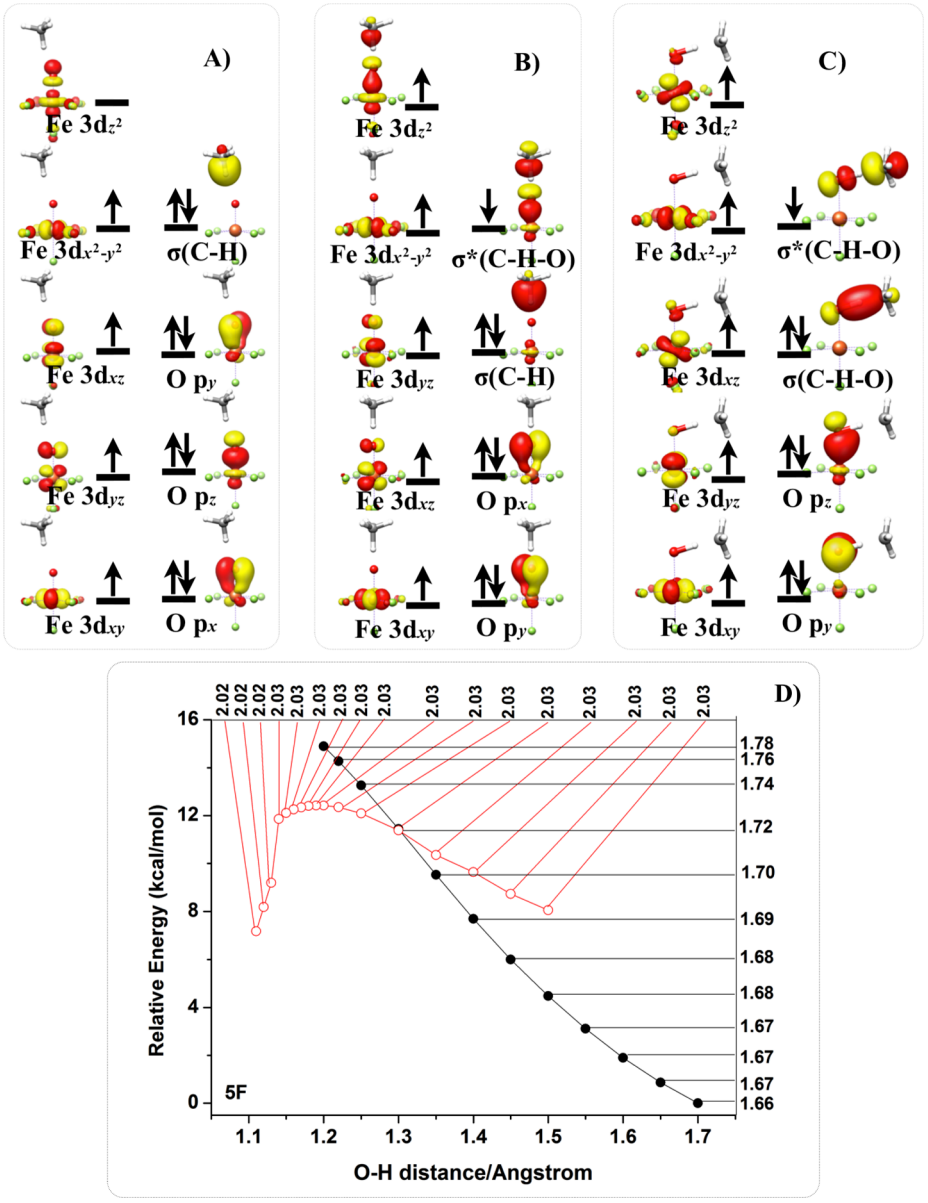

Figure 2. Schematic MO diagrams of the three structures along the quintet reaction pathway of H_3C-H approaching $[Fe^{IV}(O)(F)_5]^{3-}$. The starting complex (r(O−H) = 2.17 Å; A), r(O−H) = 1.30 Å from the black curve (B), and 1.15 Å from the red curve (C). Panel (D) shows the corresponding potential energy surfaces (pure electronic energy) as a function of the O−H distance (Å). The corresponding Fe−O bond lengths (in Å) are also shown on the right-hand for the black curve and top for the red curve in part (D).

takes place in the hybrid pathway. It follows two stages along the elongation of the Fe−O bond. First, the σ(FeO) bond is cleaved to generate the exchange-stabilized HS ferric (S_{Fe} = 5/2) center,[7] and then the π(FeO) bond is cleaved to generate a horizontally orientated electron-accepting orbital (EAO). The first stage is the same as that for the classical quintet σ-pathway.[6] However, in the classical pathway the transition state conserves the electronic structure formed in this preparatory stage (Figure 3B). On the other hand, for the hybrid pathway a second stage of Fe−O bond elongation is needed, that shifts the EAO from the vertically orientated O p_z orbital to the horizontally orientated O p_x. This transformation would result in a horizontal attack of the substrate and rationalizes the composition of the σ*(C−H−O) orbital (Figure 1). Taken these two stages together, we see that the σ-feature of this hybrid pathway, the HS ferric center, is acquired in the first stage of Fe−O bond elongation, whereas the π-character, viz. the bent Fe−O−H angle, is obtained when further elongating of Fe−O bond, favoring the horizontal attacking mode.

Similar analysis also has been dedicated to 5C and 5N systems and the corresponding data are shown in Supporting Information. For **5N**, similar results were found. As shown in Supporting Information Figure S2, the quintet surface of 5N is composed by two different potential energy curves that are similar to those found in 5F. The isolated Fe−O elongation also proves this point that two electronic states cross at about 1.86 Å (Supporting Information Figure S3). However, the result for 5C seems different. There is no evident energy difference for the top points of the two potential curves (black and red curves in Supporting Information Figure S4). Therefore, we cannot safely attribute the relative long Fe−O bond and bent Fe−O−H angle to the new features of hybrid pathway because it can also be characterized as a "late" transition state to resemble the geometry structure of product.

dx.doi.org/10.1021/jp410727r | J. Phys. Chem. B 2014, 118, 1493−1500

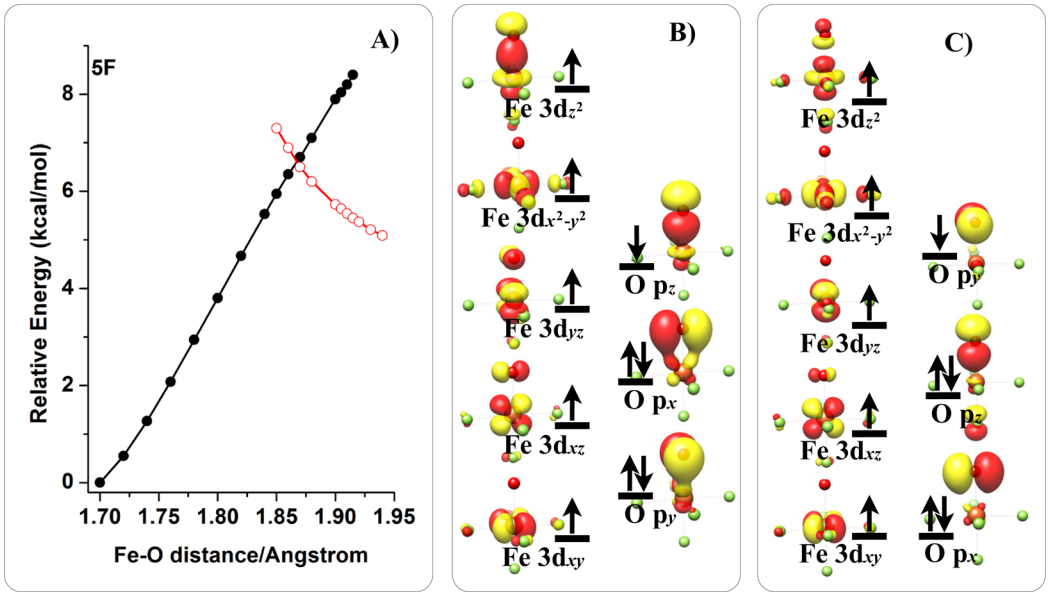

Figure 3. The quintet potential energy surfaces as a function of the Fe−O distance for $[Fe^{IV}(O)(F)_5]^{3-}$ model (A) and schematic MO diagrams at fixed Fe−O distances of 1.80 Å (B, black curve) and 1.92 Å (C, red curve).

Furthermore, the most feasible reaction pathway for this CN^- coordinated 5C system is the quintet π-pathway (blue curve in Supporting Information Figure S4), not the two pathways mentioned above. Simply elongation of the isolate Fe−O bond also proves this. As shown in Supporting Information Figure S5, the lengthening of Fe−O bond leads to a heterolytic cleavage of π(FeO), not the σ(FeO) as found in 5F and 5N systems. All these differences might be due to the π-accepting nature of CN^- ligands and systematic study on the effect of π-accepting equatorial ligands is on the way in our group.

The bent Fe−O−H angles employed in the energetically facilitated hybrid pathways in 5F and 5N are quite confusing. As has been pointed out before,[7,28] one reason why the quintet σ-pathway is more feasible than the corresponding π-pathway is that it employs the vertically directed O p_z orbital that can form an optimum orbital overlap and a minimal Pauli repulsion with the incoming substrate. Given these advantages of O p_z, why does the EAO shift from O p_z to O p_x in hybrid pathway? We can imagine at least three factors accounting for this transformation.

First, a weak π-bond between the iron center and oxo ligand would favor this shift. The weak π-bond can be obtained by introducing strong π-donating equatorial ligands. For example, the covalence of the π(FeO) bond is greatly reduced by the π-donating ligand F^- in 5F system. This is reflected by the large O contribution in the π(FeO) bonding orbital of the reactant state, 74% for O versus 27% for Fe (Table 1; cf. the classical **5A** complex, which has ∼59% O and ∼41% Fe). The Fe−O π-interaction would become even less covalent if the Fe−O bond is elongated. Therefore, the hybrid pathway will be favored if a weak π(FeO) bond is broken and a stronger σ(FeO) bond is formed. This also holds true for 5N system that bears relative weak π-donating ligands. In line with this, the π-accepting ligand CN^- demonstrates a different picture for the corresponding pathway. Second, a collinear Fe−O−H arrangement is optimum according to steric and orbital interaction considerations.[6] However, it is not the best arrangement in energy terms, because the equilibrium Fe−O−H angle is 94° for the intermediate after the transfer of the hydrogen. Given the same conditions (e.g., orbital overlap and steric hindrance) for the vertical and equatorial approach of H atom, the Fe−O−H moiety would therefore prefer a bent rather than a collinear arrangement in transition states.

Third, all the ligands employed in this study are small ions and would therefore be expected to have small steric effects, which would allow a horizontal approach of the substrate that maximizes the overlap with EAO. These three factors work together and lead to a bent Fe−O−H angle in the ideal arrangement for the quintet pathway for the coordination environments in this study. They also account for the unexpectedly high reactivity of the strongly negatively charged **5F** system with a calculated enthalpy barrier of 8 kcal/mol.

This hybrid pathway shows that the equatorial ligands also play an important role in modulating the reactivity of Fe^{IV}═O compounds as well as that found in Fe(III)-OOH system.[48,55,75] Recently, Shaik group proposed that the number of electrons in the d_{xz} orbital of the Fe^{III}−O moiety determinates the choice of the heterolytic pathway versus the homolytic pathway.[75] The weak π(FeO) bonds offer a possibility that two electronic structures of Fe−O bond are in close energy near the transition state (Figure 3). The electronic structure is partly determined by the properties of equatorial ligands. A small size of the equatorial ligands would facilitate an equatorial approach of the substrate and hence favor the hybrid pathway, whereas large equatorial ligands with enhanced steric hindrance would favor a vertical attack of the substrate and hence the classical σ-pathway (Figure 1).[6] Thus, the quintet hybrid pathway would be favored by equatorial ligands with a small size and a strong π-donating ability. This is supported by our calculations. Table 1 shows that the systems with less covalent π(FeO) bonds have low enthalpy barriers, for example, **5F** versus **2C-3F**/**2N-3F**, and **1C-4F** versus **3C-2F**. Some systems with equatorial CN^- ligands, for example, **5C**, **4C-1N**, **3C-2N**, and **2C-3N**, have a relatively strong π(FeO) bond and therefore quite high energy barriers. In addition, in our previous study the $[Fe^{IV}(O)(OH)_{2(eq)}(NH_3)_3]$ model (**3A-2O**) unexpectedly had the same reactivity as **5A** for the quintet σ-pathway (12 versus 11 kcal/mol) even though their net charge

dx.doi.org/10.1021/jp410727r | J. Phys. Chem. B 2014, 118, 1493−1500

differs by two units.[28] We attribute this enhanced reactivity of **3A-2O** to the two equatorial OH^- ligands, which reduce the covalence of the π(FeO) bonds and hence facilitate the quintet σ-pathway. The geometry parameters of the transition states are also in line with those of the present complexes. The Fe−O bond is appreciably longer in **3A-2O** (1.81 Å) than in **5A** (1.74 Å), and the **3A-2O** system features a bent Fe−O−H angle (143°), rather than the near collinear Fe−O−H arrangement found in **5A** (Table 1).[28]

CONCLUSIONS

In this paper, we have studied the nonheme Fe^{IV}=O complexes catalyzed methane C−H bond cleavage reactions with density functional theory methods. Some new features have been found in the high spin pathway, that is, the hybrid pathway. This pathway mixes features of the classical σ- (the high spin (S = 5/2) occupied ferric center) and π-pathways (the antibonding combination between the σ(C−H) and the O p_x fragment in ^{5}TSHh and the rather bent Fe−O−H angle). Our calculations also show that the equatorial ligands play key roles in tuning the reactivity of this pathway. First, the strong π-donating equatorial ligands reduce the covalence of π(FeO) bond and therefore the hybrid pathway would be facilitated by a weak π(FeO) bond broken and a stronger σ(FeO) bond formation. Second, the small size equatorial ligands would be expected to have small streic effects upon substrate approaching. Therefore, taking account these two factors the collinear Fe−O−H arrangement might not be the best choice for the quintet reactivity with small and strong π-donating equatorial ligands; instead a bent arrangement may have a higher reactivity. This work not only deepens our understanding on the C−H bond activation reactions but also directs future studies to explore equatorial ligands and steric hindrance in the design of high-valent iron-oxo complexes.

ASSOCIATED CONTENT

Supporting Information

Details of the models, relative enthalpies, calculated Cartesian coordinates of the transition states, schematic MO diagrams This material is available free of charge via the Internet at http://pubs.acs.org.

AUTHOR INFORMATION

Corresponding Author

*E-mail: Jilai@jlu.edu.cn.

Author Contributions

‖X.S. and C.G. contributed equally.

Notes

The authors declare no competing financial interest.

ACKNOWLEDGMENTS

This work was supported by the 973 program and NSFC of China (2012CB932800, 21103064), the Swedish research council (Project 2010-5025) and the Crafoord foundation.

REFERENCES

(1) Labinger, J. A.; Bercaw, J. E. *Nature* **2002**, *417*, 507.
(2) Goldberg, K. I.; Goldman, A. S. *Activation and Functionalization of C-H Bonds*; ACS Symposium Series; American Chemical Society: Washington, DC, 2004; p 885.
(3) Bergman, R. G. *Nature* **2007**, *446*, 391.
(4) Godula, K.; Sames, D. *Science* **2006**, *312*, 67.
(5) Que, L., Jr.; Tolman, W. B. *Nature* **2008**, *455*, 333.
(6) Ye, S.; Neese, F. *Proc. Natl. Acad. Sci. U.S.A.* **2011**, *108*, 1228.
(7) Shaik, S.; Chen, H.; Janardanan, D. *Nature Chem.* **2011**, *3*, 19.
(8) Nam, W. *Acc. Chem. Res.* **2007**, *40*, 522.
(9) Solomon, E. I.; Wong, S. D.; Liu, L. V.; Decker, A.; Chow, M. S. *Curr. Opin. Chem. Biol.* **2009**, *13*, 99.
(10) de Visser, S. P.; Rohde, J. U.; Lee, Y. M.; Cho, J.; Nam, W. *Coord. Chem. Rev.* **2013**, *257*, 381.
(11) McDonald, A. R.; Que, L. *Coord. Chem. Rev.* **2013**, *257*, 414.
(12) Shaik, S.; Cohen, S.; Wang, Y.; Chen, H.; Kumar, D.; Thiel, W. *Chem. Rev.* **2010**, *110*, 949.
(13) Solomon, E. I.; Brunold, T. C.; Davis, M. I.; Kemsley, J. N.; Lee, S. K.; Lehnert, N.; Neese, F.; Skulan, A. J.; Yang, Y. S.; Zhou, J. *Chem. Rev.* **2000**, *100*, 235.
(14) Shaik, S.; Hirao, H.; Kumar, D. *Acc. Chem. Res.* **2007**, *40*, 532.
(15) Krebs, C.; Fujimori, D. G.; Walsh, C. T.; Bollinger, J. M., Jr. *Acc. Chem. Res.* **2007**, *40*, 484.
(16) Ye, S.; Neese, F. *Curr. Opin. Chem. Biol.* **2009**, *13*, 89.
(17) *Iron-containing enzymes: Versatile catalysts of hydroxylation reaction in nature*; de Visser, S. P., Kumar, D., Eds.; RSC Publishing: Cambridge, U.K., 2011.
(18) *Cytochrome P450: Structure, Mechanism and Biochemistry*, 3rd ed.; Ortiz de Montellano, P. R., Ed.; Kluwer Academic/Plenum Publishers: New York, 2004.
(19) Meunier, B.; de Visser, S. P.; Shaik, S. *Chem. Rev.* **2004**, *104*, 3947.
(20) See Fe(IV) special edition of *J. Inorg. Biochem.* **2006**, *100*, and references therein.
(21) Shaik, S.; Kumar, D.; de Visser, S. P.; Altun, A.; Thiel, W. *Chem. Rev.* **2005**, *105*, 2279.
(22) Shaik, S.; de Visser, S. P.; Ogliaro, F.; Schwarz, H.; Schroder, D. *Curr. Opin. Chem. Biol.* **2002**, *6*, 556.
(23) Shilov, A. E.; Shteinman, A. A. *Acc. Chem. Res.* **1999**, *32*, 763.
(24) Que, L., Jr. *Acc. Chem. Res.* **2007**, *40*, 493.
(25) Yoshizawa, K. *Coord. Chem. Rev.* **2002**, *226*, 251.
(26) Cho, J.; Jeon, S.; Wilson, S. A.; Liu, L. V.; Kang, E. A.; Braymer, J. J.; Lim, M. H.; Hedman, B.; Hodgson, K. O.; Valentine, J. S.; Solomon, E. I.; Nam, W. *Nature* **2011**, *478*, 502.
(27) Sastri, C. V.; Lee, J.; Oh, K.; Lee, Y. J.; Lee, J.; Jackson, T. A.; Ray, K.; Hirao, H.; Shin, W.; Halfen, J. A.; Kim, J.; Que, L., Jr.; Shaik, S.; Nam, W. *Proc. Natl. Acad. Sci. U.S.A.* **2007**, *104*, 19181.
(28) Geng, C. Y.; Ye, S.; Neese, F. *Angew. Chem., Int. Ed.* **2010**, *49*, 5717.
(29) Li, J. L.; Zhang, X.; Huang, X. R. *Phys. Chem. Chem. Phys.* **2012**, *14*, 246.
(30) Sun, X.-L.; Huang, X.-R.; Li, J.-L.; Huo, R.-P.; Sun, C.-C. *J. Phys. Chem. A* **2012**, *116*, 1475.
(31) Decker, A.; Rohde, J.; Klinker, E. J.; Wong, S. D.; Que, L., Jr.; Solomon, E. I. *J. Am. Chem. Soc.* **2007**, *129*, 15983.
(32) Hoffart, L. M.; Barr, E. W.; Guyer, R. B.; Bollinger, J. M., Jr.; Krebs, C. *Proc. Natl. Acad. Sci. U.S.A.* **2006**, *103*, 14738.
(33) Lehnert, N.; Neese, F.; Ho, R. Y.; Que, L., Jr.; Solomon, E. I. *J. Am. Chem. Soc.* **2002**, *124*, 10810.
(34) de Visser, S. P. *J. Am. Chem. Soc.* **2010**, *132*, 1087.
(35) Altun, A.; Shaik, S.; Thiel, W. *J. Am. Chem. Soc.* **2007**, *129*, 8978.
(36) Kumar, D.; Hirao, H.; Que, L., Jr.; Shaik, S. *J. Am. Chem. Soc.* **2005**, *127*, 8026.
(37) Hirao, H.; Kumar, D.; Thiel, W.; Shaik, S. *J. Am. Chem. Soc.* **2005**, *127*, 13007.
(38) Bassan, A.; Blomberg, M. R. A.; Siegbahn, P. E. M.; Que, L. *Angew. Chem., Int. Ed.* **2005**, *44*, 2939.
(39) Chung, L. W.; Li, X.; Hirao, H.; Morokuma, K. *J. Am. Chem. Soc.* **2011**, *133*, 20076.
(40) Schwarz, H. *Angew. Chem., Int. Ed.* **2011**, *50*, 10096.
(41) Kumar, D.; Sastry, G. N.; de Visser, S. P. *J. Phys. Chem. B* **2012**, *116*, 718.
(42) Rittle, J.; Green, M. T. *Science* **2010**, *330*, 933.

(43) Rohde, J. U.; In, J. H.; Lim, M. H.; Brennessel, W. W.; Bukowski, M. R.; Stubna, A.; Münck, E.; Nam, W.; Que, L., Jr. *Science* **2003**, *299*, 1037.
(44) Van Heuvelen, K. M.; Fiedler, A. T.; Shan, X.; De Hont, R. F.; Meier, K. K.; Bominaar, E. L.; Munck, E.; Que, L., Jr. *Proc. Natl. Acad. Sci. U.S.A.* **2012**, *109*, 11933.
(45) Siegbahn, P. E. M.; Borowski, T. *Acc. Chem. Res.* **2006**, *39*, 729.
(46) Ensing, B.; Buda, F.; Gribnau, M. C. M.; Baerends, E. J. *J. Am. Chem. Soc.* **2004**, *126*, 4355.
(47) de Visser, S. P. *J. Am. Chem. Soc.* **2006**, *128*, 9813.
(48) Bernasconi, L.; Louwerse, M. J.; Baerends, E. J. *Eur. J. Inorg. Chem.* **2007**, 3023.
(49) Neidig, M. L.; Decker, A.; Choroba, O. W.; Huang, F.; Kavana, M.; Moran, G. R.; Spencer, J. B.; Solomon, E. I. *Proc. Natl. Acad. Sci. U.S.A.* **2006**, *103*, 12966.
(50) Gonzalez-Ovalle, L. E.; Quesne, M. G.; Kumar, D.; Goldberg, D. P.; de Visser, S. P. *Org. Biomol. Chem.* **2012**, *10*, 5401.
(51) Kumar, D.; Sastry, G. N.; de Visser, S. P. *Chem.—Eur. J.* **2011**, *17*, 6196.
(52) de Visser, S. P.; Latifi, R.; Tahsini, L.; Nam, W. *Chem. Asian J.* **2011**, *6*, 493.
(53) de Visser, S. P.; Tahsini, L.; Nam, W. *Chem.—Eur. J.* **2009**, *15*, 5577.
(54) Takahashi, A.; Yamaki, D.; Ikemura, K.; Kurahashi, T.; Ogura, T.; Hada, M.; Fujii, H. *Inorg. Chem.* **2012**, *51*, 7296.
(55) Bernasconi, L.; Baerends, E. J. *Eur. J. Inorg. Chem.* **2008**, 1672.
(56) Rohde, J. U.; Stubna, A.; Bominaar, E. L.; Munck, E.; Nam, W.; Que, L., Jr. *Inorg Chem* **2006**, *45*, 6435.
(57) Bordwell, F. G.; Cheng, J. P.; Ji, G. Z.; Satish, A. V.; Zhang, X. M. *J. Am. Chem. Soc.* **1991**, *113*, 9790.
(58) Mayer, J. M. *Acc. Chem. Res.* **1998**, *31*, 441.
(59) Neese, F. *Comput. Mol. Sci.* **2012**, *2*, 73.
(60) Becke, A. D. *J. Chem. Phys.* **1993**, *98*, 5648.
(61) Kim, K.; Jordan, K. D. *J. Phys. Chem.* **1994**, *98*, 10089.
(62) Schafer, A.; Huber, C.; Ahlrichs, R. *J. Chem. Phys.* **1994**, *100*, 5829.
(63) Neese, F.; Wennmohs, F.; Hansen, A.; Becker, U. *Chem. Phys.* **2009**, *356*, 98.
(64) Weigend, F.; Haser, M.; Patzelt, H.; Ahlrichs, R. *Chem. Phys. Lett.* **1998**, *294*, 143.
(65) Weigend, F.; Kohn, A.; Hattig, C. *J. Chem. Phys.* **2002**, *116*, 3175.
(66) Klamt, A.; Schuurmann, G. *Perkin. Trans.* **1993**, 799.
(67) Grimme, S.; Antony, J.; Ehrlich, S.; Krieg, H. *J. Chem. Phys.* **2010**, 132.
(68) Grimme, S.; Ehrlich, S.; Goerigk, L. *J. Comput. Chem.* **2011**, *32*, 1456.
(69) Lundberg, M.; Siegbahn, P. E. *J. Chem. Phys.* **2005**, *122*, 224103.
(70) Janardanan, D.; Usharani, D.; Chen, H.; Shaik, S. *J. Phys. Chem. Lett* **2011**, *2*, 2610.
(71) Kamachi, T.; Yoshizawa, K. *J. Am. Chem. Soc.* **2003**, *125*, 4652.
(72) Tahsini, L.; Bagherzadeh, M.; Nam, W.; de Visser, S. P. *Inorg. Chem.* **2009**, *48*, 6661.
(73) Hirao, H.; Que, L., Jr.; Nam, W.; Shaik, S. *Chem.—Eur. J.* **2008**, *14*, 1740.
(74) Hirao, H.; Kumar, D.; Que, L., Jr.; Shaik, S. *J. Am. Chem. Soc.* **2006**, *128*, 8590.
(75) Kim, Y. M.; Cho, K.-B.; Cho, J.; Wang, B.; Li, C.; Shaik, S.; Nam, W. *J. Am. Chem. Soc.* **2013**, *135*, 8838.